Utility of quantitative measurement of T_2 using Restriction Spectrum Imaging for detection of clinically significant prostate cancer

Mariluz Rojo Domingo*[1,2], Christopher C Conlin, PhD*[3], Roshan A Karunamuni, PhD[2], Courtney Ollison, BS[2], Madison T Baxter, MS[2], Karoline Kallis, PhD[2], Deondre D Do, BS[1,2], Yuze Song, MS[2,4], Joshua M Kuperman, PhD[3], Ahmed S Shabaik, MD[5], Michael E Hahn, MD ,PhD[3], Paul M Murphy, MD, PhD[3], Rebecca Rakow-Penner, MD, PhD[3], Anders M Dale, PhD[3,6,7], Tyler M Seibert, MD, PhD[1,2,3]

*These authors contributed equally to this work

[1]Department of Bioengineering, UC San Diego Jacobs School of Engineering, La Jolla, CA, USA

[2]Department of Radiation Medicine and Applied Sciences, UC San Diego School of Medicine, La Jolla, CA, USA

[3]Department of Radiology, UC San Diego School of Medicine, La Jolla, CA, USA

[4]Department of Electrical and Computer Engineering, UC San Diego Jacobs School of Engineering, La Jolla, CA, USA

[5]Department of Pathology, UC San Diego School of Medicine, La Jolla, CA, USA

[6]Department of Neurosciences, UC San Diego School of Medicine, La Jolla, CA, USA

[7]Halıcıoğlu Data Science Institute, UC San Diego, La Jolla, CA, USA

Abstract

Background. The Restriction Spectrum Imaging restriction score (RSIrs) has demonstrated higher diagnostic accuracy for clinically significant prostate cancer (csPCa) than conventional DWI. Both diffusion and T_2 properties of prostate tissue inform the RSI signal, and studies have shown that each may be valuable for csPCa discrimination.

Purpose. To determine whether prostate T_2 varies across RSI compartments and in the presence of csPCa, and to evaluate whether consideration of compartmental T_2 (cT_2) improves csPCa detection over RSIrs alone.

Study Type. Retrospective.

Population. Two cohorts (46 and 195 patients) scanned for csPCa.

Field Strength/Sequence. 3T multi-*b*-value DWI acquired at multiple TEs.

Assessment. cT_2 values were computed from multi-TE RSI data and compared between RSI model compartments. csPCa detection was compared between RSIrs and a logistic regression model (LRM) for predicting the probability of csPCa using cT_2 in combination with RSI measurements.

Statistical Tests. *T*wo-sample t-tests (α=0.05) were used to compare cT_2 values between compartments and between patients with and without csPCa. Area under the receiver operating characteristic curve (AUC) was used to evaluate csPCa detection performance.

Results. In both cohorts, T_2 differed (p<0.05) across all RSI compartments (C_1, C_2, C_3, C_4). Voxel-level data from cohort 1 showed that T_2 differed between normal and cancerous tissue in C_1, C_2, C_3 (p<0.001). Whole-prostate T_2 differed between patients with and without csPCa in C_3 (p=0.02). In cohort 2, whole-prostate T_2 differed in C_1 (p=0.01), C_3 (p=0.01), and C_4 (p<0.01). Consideration of cT_2 improved csPCa discrimination compared to diffusion alone, but not compared to RSIrs [cohort 1: 0.80 vs 0.70 (diffusion) and 0.80 (RSIrs), cohort 2: 0.72 vs 0.65 (diffusion) and 0.72 (RSIrs)].

Data Conclusion. Significant differences in cT_2 were observed between normal and cancerous prostatic tissue. With our data, however, consideration of cT_2 did not significantly improve cancer detection performance over RSIrs alone.

Keywords

Prostate; Cancer detection; T_2 mapping; Restriction Spectrum Imaging; Diffusion-Weighted Imaging

Introduction

Multiparametric magnetic resonance imaging (mpMRI) has become an important tool for the diagnosis of prostate cancer (PCa)[1]. MpMRI has proven to reduce unnecessary biopsies, mitigates overdiagnosis of clinically insignificant prostate cancer (indolent PCa), and enhances detection of clinically significant prostate cancer (csPCa, Grade Group 2 or higher)[2,3]. In standard reporting of prostate MRI (Prostate Imaging Reporting and Data System, PI-RADS v2.1[4]), diffusion-weighted imaging (DWI) and T_2 -weighted imaging are the principal modalities used to detect csPCa. DWI measures the random movement of water molecules within tissues, aiding in the visualization of areas of restricted diffusion associated with hypercellular csPCa[5]. Meanwhile, T_2 -weighted imaging provides detailed anatomical information and facilitating the visualization of abnormalities in prostate tissue. The combined analysis of these two sequences allows for a more in-depth evaluation of potential tumor lesions, thereby contributing to csPCa detection and characterization.

The challenge with the interpretation of conventional mpMRI lies in its inherent subjectivity and variability[6]. The interpretations of imaging data by different radiologists that rely on qualitative assessment alone leads to inconsistencies in the identification and characterization of csPCa lesions[7]. Interobserver variability significantly limits the accuracy and reliability of csPCa diagnosis[8]. To enhance diagnostic accuracy, there is a growing emphasis on the development and adoption of quantitative MRI approaches. Quantitative MRI aims to provide objective metrics of tissue properties associated with the probability of csPCa, offering the potential for more standardized and reproducible image assessment.

Restriction Spectrum Imaging (RSI) is a quantitative approach to DWI for csPCa detection and characterization. RSI scans are acquired at multiple *b*-values (diffusion weightings) to distinguish diffusion signal from tissue micro-compartments (intracellular water, extracellular hindered water, freely diffusing water, and flowing fluid)[9–12]. However, RSI models typically do not incorporate quantitative T_2 measurements. On the other hand, studies using luminal water imaging (LWI) and hybrid multidimensional MRI

have shown that tissue T_2 can differ between prostate tissue compartments and provide diagnostic information that is complementary to diffusion[13,14].

In this study, we acquired prostate RSI data at multiple echo times (TEs) to measure compartmental T_2 in addition to diffusion. We aimed to determine whether compartmental T_2 (i.e., T_2 within each RSI micro-compartment) differs between cancerous and normal prostate tissue, and whether consideration of compartmental T_2 in RSI yields improved detection of csPCa.

Methods

Study Population

This study was approved by the institutional review board (IRB). For the prospective cohort, a waiver of consent was obtained to acquire images with two TEs for image optimization, as well as to access patient images and other clinical information. Consecutive patients of age 18 years or older who underwent MRI with multi-TE RSI for suspected PCa were included in the two cohorts of this study. The first cohort (retrospective) included patients scanned for PCa between August and December of 2016 with multi-TE RSI as part of a quality improvement project. The second cohort included patients who were scanned for PCa between March 2021 and January of 2023. Additionally, the second cohort included participants in a separate, prospective study (also approved by the IRB) of patients with localized prostate cancer using the same multi-TE RSI protocol. These latter participants gave informed consent to undergo additional imaging before and after radiation therapy; only pre-treatment imaging was included in the present study. Patients were excluded if they had received any treatment for PCa prior to the MRI acquisition or if a lesion with PI-RADS score ≥3 was detected on MRI but no biopsy information was available.

Routine Clinical Evaluation

Most patients in both cohorts underwent prostate MRI as part of routine clinical care for PCa. MpMRI was performed according to PI-RADS guidelines, and interpretation was made per clinical routine using PI-RADS v2.1. Several patients, all from cohort 2, had

PCa diagnosed on systematic biopsy without MRI, and then had an MRI with RSI before any treatment as part of a prospective study; PI-RADS scores are not available for these subjects. The presence of clinically significant prostate cancer (csPCa, grade group 2 or higher) was determined from the best available histopathology, either biopsy (typically systematic 12-core biopsy with additional targeted cores for suspicious lesions on MRI) or radical prostatectomy. Patients with PI-RADS lesions of 1 or 2 with no biopsy were considered negative for csPCa, in accordance with European Association of Urology (EAU) guidelines[15–17].

RSI Data Acquisition and Processing

All patients were scanned with an expanded MRI protocol that included two multi-*b*-value RSI acquisitions performed with different TEs. MRI acquisition details are summarized in Table 1. All MR imaging was performed on a 3T clinical scanner (Discovery MR750; GE Healthcare, Waukesha, WI, USA), using a 32-channel phased-array coil over the pelvis. For each patient, two axial, multi-*b*-value DWI volumes were separately acquired using two different TEs: 80 ms and 100 ms for cohort 1, and 76 ms and 90 ms for cohort 2. The other parameters were the same between scans. In addition to the DWI volumes, a single T_2-weighted volume was acquired for anatomical reference using the same scan coverage as the DWI volumes. MRI post-processing was performed using programs implemented in MATLAB (MathWorks, Natick, MA, USA). DWI volumes were corrected to account for B_0-inhomogeneities, gradient nonlinearities, eddy currents[18], and image noise[10]. Samples at each *b*-value were averaged together. Image registration[19] was applied to correct for patient motion between acquisitions.

Cohort 1	DWI 1	DWI 2	T_2-weighted
Pulse sequence	Diffusion-weighted EPI*	Diffusion-weighted EPI*	FSE†
TR (ms)	5000	5000	6225
TE (ms)	80	100	100
FOV (mm)	220	220	220
Matrix [resampled dimensions]	96 x 96 x [128 x 128]	96 x 96 x [128 x 128]	320 x 320 x [512 x 512]
Slices	34	34	34
Slice Thickness (mm)	3	3	3
b -values (s/mm^2) [number of samples]	0[7‡], 200 [6], 1000 [6], 2000 [6], 3000 [6]	0[7‡], 200 [6], 1000 [6], 2000 [6], 3000 [6]	N/A

*Echo-planar imaging
†Fast spin echo
‡An extra b = 0 s/mm2 volume was acquired with reverse phase encoding to enable correction of B0-inhomogeneity distortions

Cohort 2	DWI 1	DWI 2	T_2-weighted
Pulse sequence	Diffusion-weighted EPI*	Diffusion-weighted EPI*	FSE†
TR (ms)	4500	4500	6230
TE (ms)	76	90	98
FOV (mm)	200 x 100	200 x 100	200 x 200
Matrix [resampled dimensions]	80 x 48 x [128 x 128]	80 x 48 x [128 x 128]	320 x 320 x [512 x 512]
Slices	32	32	32
Slice Thickness (mm)	3	3	3
b -values (s/mm^2) [number of samples]	0 [2‡], 50[6], 800[6], 1500[12], 3000 [18]	0 [2‡], 50[6], 800[6], 1500[12], 3000 [18]	N/A

*Echo-planar imaging
†Fast spin echo
‡An extra b = 0 s/mm2 volume was acquired with reverse phase encoding to enable correction of B0-inhomogeneity distortions

Table 1: Acquisition details for DWI and T_2-weighted image volumes. All MR imaging was performed on a 3T clinical scanner (Discovery MR750; GE Healthcare), using a 32-channel phased-array coil over the pelvis. The two DWI volumes for both cohorts were acquired using different TEs to allow for examination of T_2 relaxation in prostatic tissue compartments. The single T_2-weighted volume was acquired for anatomical reference.

For patients in cohort 1, regions of interest (ROIs) were manually defined on T_2-weighted images over the whole prostate, peripheral zone, and transition zone (the central zone was included with the transition zone). The contouring of the prostate zones and tumor lesions was performed using MIM software (MIM Software, Inc;

Cleveland, OH, USA), by a radiation oncologist with 3 years of experience and two board-certified sub-specialist radiologists with 4 and 6 years of experience, using all available clinical imaging and pathologic information[11]. Radiologist-certified contours of the prostate zones and lesions were not obtainable for cohort 2. Instead, contours of the whole prostate were generated automatically using OnQ Prostate software from Cortechs Labs (Cortech.ai; San Diego, CA, USA).

RSI modeling

Prior studies established and validated a four-compartment RSI model of the diffusion signal[10,11,20]:

$$S(b) = \sum_{i=1}^{4} C_i e^{-bD_i}$$

S(b) denotes the measured DWI signal intensity at a particular *b*-value, which is modeled as a linear combination of exponential decays representing four diffusion compartments. C_i describes the compartmental signal contributions to be determined via model-fitting. The diffusion coefficients, D_i, are fixed for each of the four tissue compartments to empirically determined[10] values that broadly represent restricted, hindered, free diffusion, and vascular flow: 1.1e-4, 1.8e-3, 3.6e-3, and 0.1220 mm^2/s, respectively. Signal-contribution (C_i) maps were computed for both DWI volumes per patient by fitting this model to the signal-vs.-*b*-value curve from each voxel. A previously validated biomarker for PCa called the RSI restriction score (RSIrs) was computed by dividing the signal intensity of the restricted diffusion compartment, C_1, at each voxel by the median signal intensity within the whole prostate on the $b = 0$ mm^2/s DWI images (an index of apparent T_2-weighting in the prostate)[11,20–23].

Compartmental T_2 mapping and analysis by csPCa status

T_2 maps were computed for each compartment of the RSI model by fitting the monoexponential T_2 decay formula to the signal values from the two C_i maps with different TEs. The median T_2 within the whole prostate was then computed. Two-sample

t-tests (α = 0.05) were used to determine whether there were significant differences in median T_2 between compartments.

For cohort 1, two-sample *t*-tests (α = 0.05) were used to compare median compartmental T_2 values between benign or clinically insignificant PCa tissue and csPCa lesions. For both cohorts, we used two-sample *t*-tests (α = 0.05) to compare each patient's median T_2 by compartment in the whole prostate, and whether compartmental T_2 was significantly different between patients with and without csPCa. Any compartments with a significant difference in T_2 between normal and cancerous tissue were noted for inclusion in subsequent multivariable modeling.

<u>Logistic regression model fitting and evaluation of cancer-detection performance</u>

A logistic regression model (LRM) was developed to estimate the probability that a given voxel of tissue contains csPCa given measurements of diffusion and compartmental T_2. RSIrs[11] was included as the diffusion parameter of the model. Compartmental T_2 was included in the LRM for each compartment that showed a significant difference in T_2 between normal and cancerous tissue. Cohort 1 had radiologist-certified lesion contours available and was therefore used to train the LRM. In patients with csPCa, voxels inside the lesion contours were labeled as csPCa-positive, while prostate voxels outside the lesion contours were labeled as csPCa-negative. In these patients, voxels labeled as csPCa-positive were included to train the LRM and all non-csPCa voxels were excluded. In patients without csPCa, diffusion and compartmental T_2 measurements from all voxels within the entire prostate were used to train the LRM and labeled as csPCa-negative.

Ten-fold cross-validation was performed to evaluate voxel-level csPCa-detection performance of the model within cohort 1. We assessed csPCa-detection performance using the area under the receiver operating characteristic curve (AUC) and calculated 95% confidence intervals (CI) from 10,000 bootstrap samples.

Both cohorts were used to test the patient-level csPCa-detection performance of the model. For patient-level analysis of the LRM, the highest probability value observed within the whole prostate was used as the predictor variable. Similarly, the maximum RSIrs value within the whole prostate was used as the patient-level predictor for RSIrs. We also computed maximum C_1 to obtain the patient-level performance of diffusion only, as RSIrs incorporates global prostate T_2 signal in addition to diffusion signal. AUC values were computed for maximum C_1, maximum RSIrs, and the LRM, and compared using two-sample *t*-tests ($\alpha = 0.05$). The 95% confidence intervals were estimated through random sampling with replacement from 10,000 bootstrap patient samples.

Results

Study Population

Cohort 1 comprised 46 patients (age: 70 ± 10 years; PSA: 10.6 ±16.9 ng/mL). Cohort 2 comprised 195 patients (age: 69 ± 8 years; PSA: 8.2 ± 8.5 ng/mL). In cohort 1, 22 of 46 patients (47.8%) had csPCa, while the remaining 24 had either low-grade (grade group 1) disease or no cancer. In cohort 2, 96 of 195 (49.2%) patients had csPCa. 38 participants from cohort 2 had no PI-RADS scores available because csPCa was diagnosed on systematic biopsy without MRI and then had an MRI with RSI acquisition as part of a separate, prospective study. Table 2 summarizes the patient characteristics of both cohorts.

Cohort 1 (n = 46)		
Available Pathology	Systematic biopsy only	6
	Targeted Biopsy Only	0
	Systematic and targeted biopsy	20
	Prostatectomy	15
	No biopsy or prostatectomy*	5
PI-RADS	1	9
	2	2
	3	10
	4	10
	5	15
	Not available	0
Gleason Grade Group	Benign	17
	1	2
	2	9
	3	8
	4	1
	5	4

*4 patients had PI-RADS 1 scores and 1 patient had PI-RADS 2 scores.

Cohort 2 (n = 195)		
Available Pathology	Systematic biopsy only	44
	Targeted Biopsy Only	5
	Systematic and targeted biopsy	60
	Prostatectomy	28
	No biopsy or prostatectomy*	31
PI-RADS	1	66
	2	10
	3	18
	4	36
	5	27
	Not available†	38
Gleason Grade Group	Benign	38
	1	30
	2	40
	3	32
	4	7
	5	17

*27 patients had PI-RADS 1 scores and 4 patient had PI-RADS 2 scores.

†Part of a prospective research study without clinical evaluation by a radiologist

Table 2. Summary of radiologic and pathologic characteristics of the two cohorts of patients included in this study.

Compartmental T_2 mapping

Figure 1 shows compartmental T_2 maps for two patients with csPCa, one from each cohort.

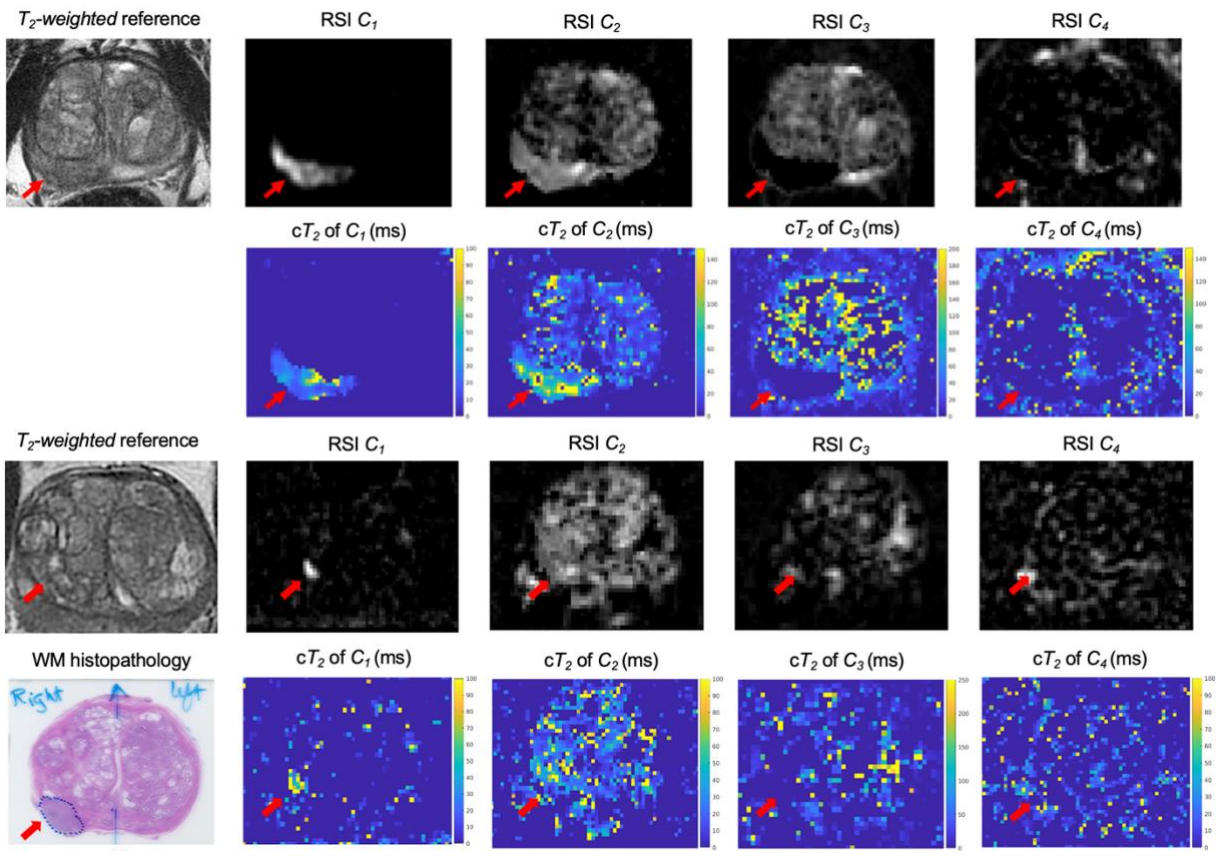

Figure 1: RSI signal contribution (C_i) and compartmental T_2 (cT_2) maps for two patients with csPCa. The top panel corresponds to a patient from cohort 1 and the bottom panel to a patient from cohort 2. Compartmental T_2 maps were computed for each RSI model compartment by measuring the T_2 -weighted signal decay of the signal-contribution map for different TEs. The signal-contribution maps shown here were computed from the DWI acquisition with shorter TE. Whole-mount (WM) histopathology results were available for the patient from cohort 2 and illustrate the lesion contour in the prostate.

Figure 2 shows violin plots of median T_2 within the whole prostate for each RSI model compartment. In both cohorts, the highest median T_2 values were observed in C_3, followed by C_2, C_4, and finally C_1. Compartmental T_2 was significantly different between any two compartments ($p < 0.05$).

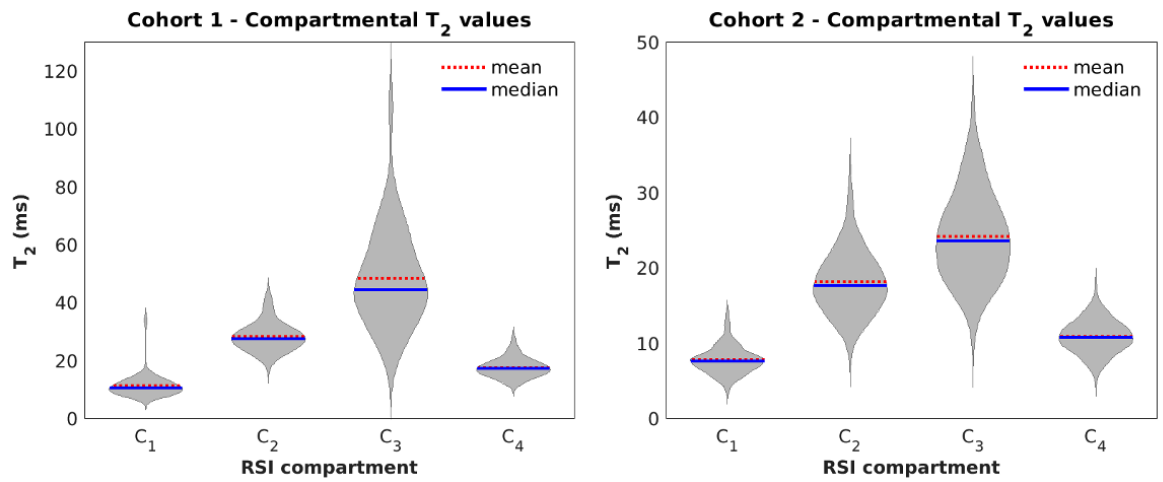

Figure 2: Violin plots showing the distribution of median T_2 values in the whole prostate for each of the four RSI model compartments. Within each cohort, compartmental T_2 was significantly different between any two compartments ($p < 0.05$). Left panel: cohort 1 (n = 46). Right panel: cohort 2 (n = 195).

<u>Voxel-level analysis of compartmental T_2 values by csPCa status</u>

For each compartment of the RSI model, the comparison of T_2 values between csPCa and prostate tissue outside of csPCa lesions is illustrated in Figure 3. This figure corresponds to cohort 1, which has radiologist-certified csPCa lesion contours. csPCa lesions showed significantly higher compartmental T_2 values in compartment 1 (p-value << 0.001) and compartment 2 (p-value << 0.001) than normal tissue. In addition, the compartmental T_2 values of compartment C_3 were significantly lower in csPCa lesions (p-value << 0.001). The compartmental T_2 values for compartment C_4 were not significantly different between csPCa and normal tissues (p-value = 0.17).

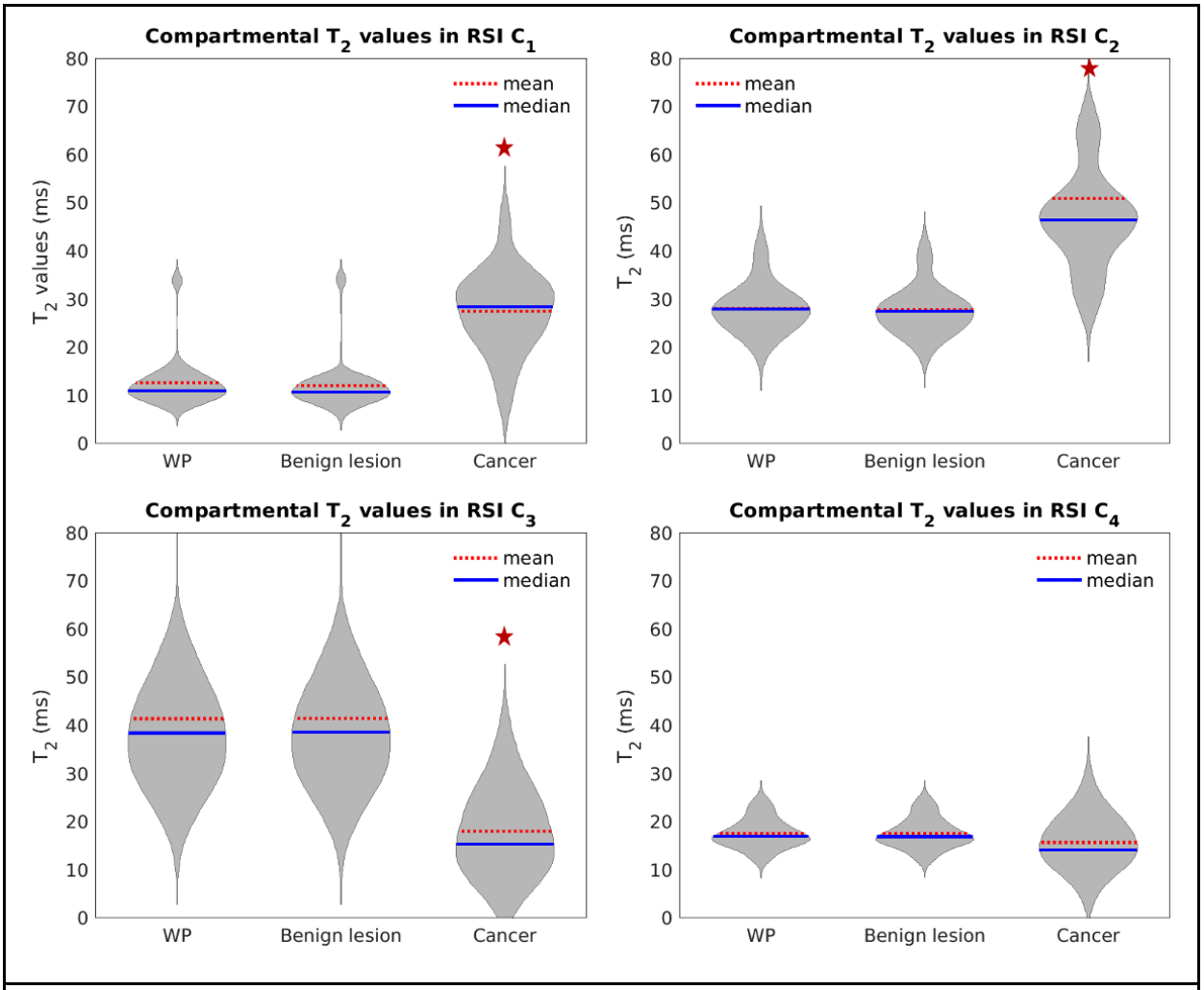

Figure 3: Violin plots showing the distribution of median compartmental T_2 values from cohort 1 in both csPCa lesions and the surrounding prostate tissue. The red "+" corresponds to the mean value in each violin. Each panel corresponds to one of the RSI diffusion compartments. csPCa lesions showed significantly higher compartmental T2 values in C_1 (p-value << 0.001) and C_2 (p-value << 0.001) than tissues outside of csPCa lesions. Compartmental T_2 values of C_3 were also significantly lower in csPCa lesions than outside csPCa lesions (p-value << 0.001). A red star indicates a significant difference (p-value < 0.05) in compartmental T_2 between csPCa lesions and the prostate tissue outside the lesions. WP: whole prostate.

<u>Patient-level analysis of compartmental T_2 values by csPCa status</u>

The comparison of compartmental T_2 values between patients with and without csPCa is shown in Figure 4. In both cohorts, patients with csPCa had higher compartmental T_2 values in compartment C_1 than patients with no csPCa. In cohort 2, median C_1 compartmental T_2 was significantly higher (p-value = 0.07 for cohort 1; p-value = 0.01 for cohort 2). Median C_3 compartmental T_2 was significantly different between csPCa and patients without csPCa in both cohorts (p-value = 0.02 for cohort 1; p-value = 0.01 for cohort 2). Median C_4 compartmental T_2 was also significantly different in cohort 2 (p-value << 0.01). Compartmental T_2 values for the other compartments were not significantly different between patients with and without csPCa.

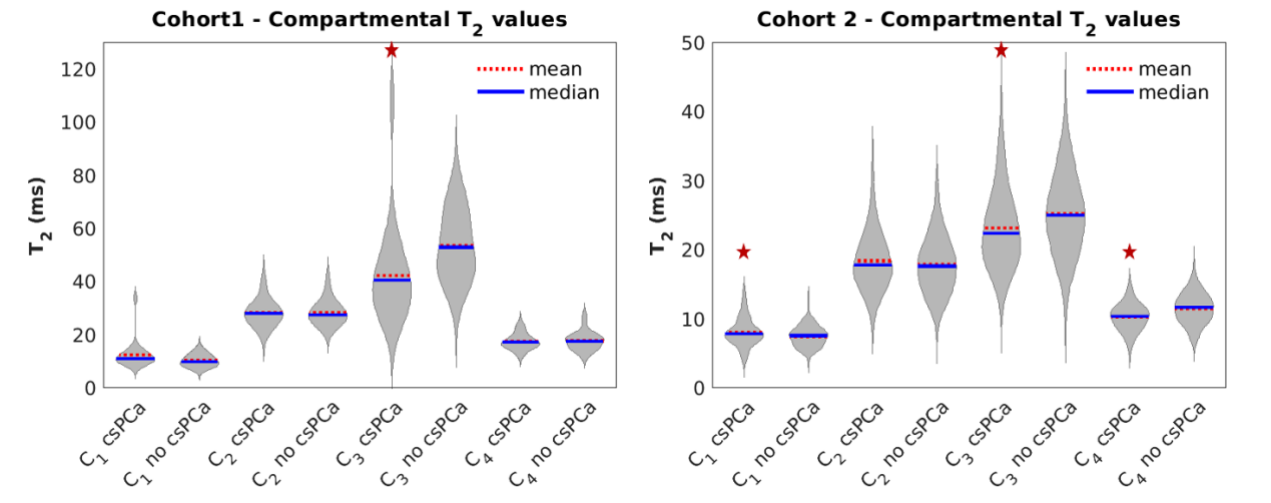

Figure 4: Violin plots comparing compartmental T_2 within the whole prostate between patients with csPCa and those without. A red star indicates a significant difference (p-value < 0.05) in whole-prostate compartmental T_2 between csPCa and non-csPCa patients. Left panel: cohort 1 (n = 46). Right panel: cohort 2 (n = 195).

<u>Logistic regression model fitting and evaluation of csPCa-detection performance</u>

T_2 measurements from RSI compartments 1, 2, and 3 (C_1, C_2, C_3) were included as the T_2 parameters of the LRM. These three compartments showed significantly different median T_2 signal between in csPCa lesions vs csPCa-negative voxels. The LRM predictors were RSIrs, C_1 T_2 , C_2 T_2, and C_3 T_2. The model coefficients with 95% confidence interval for the y-intercept and RSIrs were 6.367 (6.323, 6.416) and -51.621

(-52.354, -50.888), respectively. The weights for $C_1\ T_2$, $C_2\ T_2$, and $C_3\ T_2$ were < 0.005. Example probability maps computed from the model are shown in Figure 5 for two patients with csPCa, alongside maps of RSIrs.

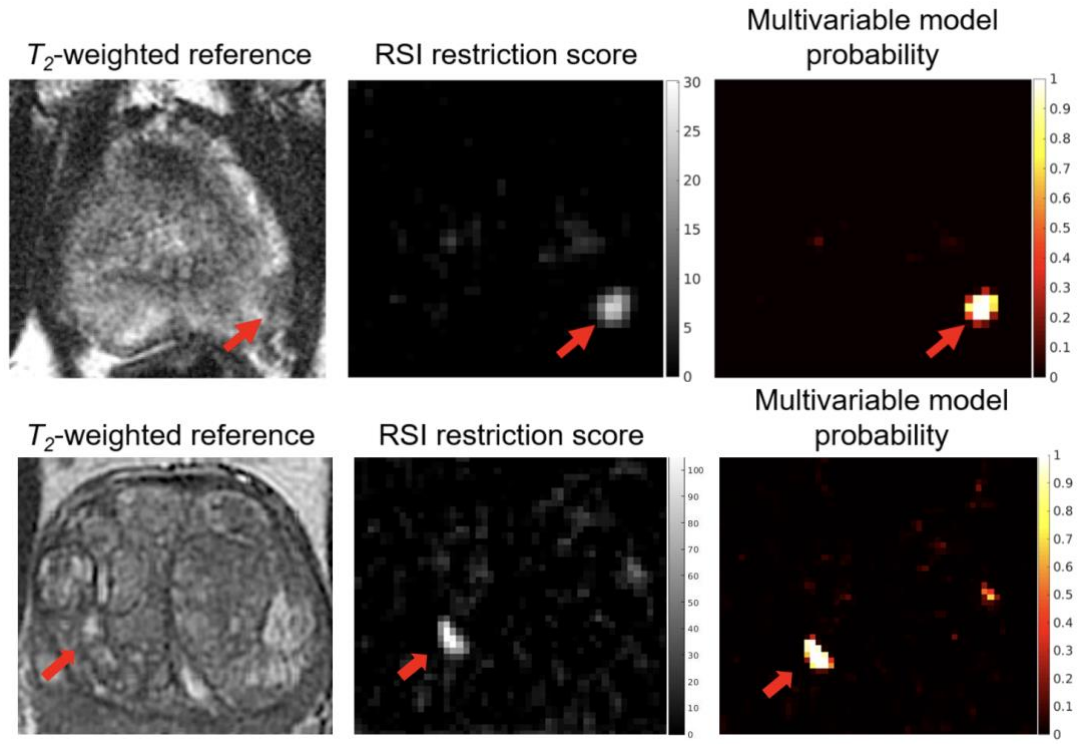

Figure 5: RSI restriction score and multivariable model probability maps of the prostate for patients with csPCa. Top panel: Patient from cohort 1 with a lesion in the left peripheral zone. Bottom panel: Patient from cohort 2 with a lesion in the transition zone. The multivariable model uses compartmental T_2 measurements from each voxel in addition to the RSI restriction score to determine the probability that it contains csPCa.

<u>Voxel-level cancer detection</u>

For voxel-level cancer detection, the 10-fold cross-validation mean AUC of the LRM was 0.98 [95% CI: 0.957, 0.985], versus 0.98 [95% CI: 0.958, 0.986] for maximum RSIrs, indicating that incorporating compartmental T_2 did not improve discrimination over RSIrs alone (p-value = 0.9).

Patient-level cancer detection

For cohort 1, the AUC of the LRM was 0.804 [0.648,0.930], versus 0.805 [0.648, 0.931] for RSIrs. The mean AUC for maximum C_1 was 0.695 [0.530, 0.851]. The difference in AUCs between RSIrs and the multivariable model was not significantly different (*p*-value = 0.26). Both RSIrs and the LRM performed significantly better than diffusion (maximum C_1) alone (both *p*-values << 0.001).

For cohort 2, the mean LRM AUC for 10,000 bootstrapped samples was 0.724 [0.650, 0.793]. The mean AUC of RSIrs for 10,000 bootstrapped samples was 0.725 [0.652, 0.794]. For maximum C_1 the mean AUC was 0.654 [0.573,0.730].
The difference in AUCs between RSIrs and the multivariable model was not significantly different (*p*-value = 0.54). Both RSIrs and the LRM performed significantly better than diffusion (maximum C_1) alone (both *p*-values << 0.001).

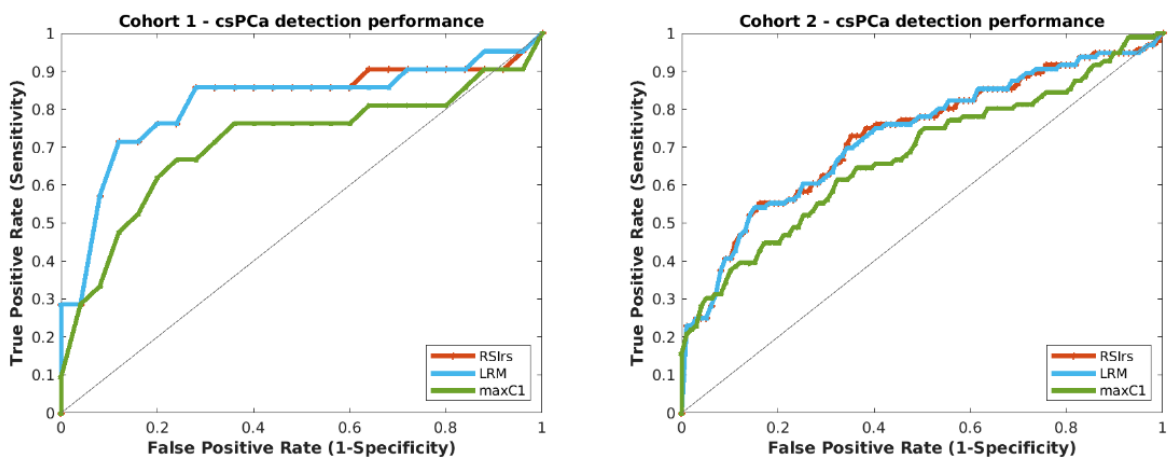

Figure 5: Patient-level diagnostic performance of maximum RSIrs, the LRM and maximum C_1 (max C_1) for cohorts 1 and 2. For cohort 1, mean AUC values were 0.695 for maximum C_1, 0.805 for RSIrs and 0.804 for the multivariable model. For cohort 2, mean AUC values were 0.654 for maximum C_1, 0.725 for RSIrs and 0.724 for the multivariable model.

Discussion

We found that compartmental T_2 values were significantly different across RSI diffusion compartments. Moreover, compartmental T_2 values differed between csPCa lesions and benign tissue or low-grade PCa in compartments C_1, C_2, and C_3. At the patient level, there were also differences in whole-prostate T_2 between patients with no csPCa and those with biopsy-proven csPCa. Quantitative differences in compartmental T_2 may provide insight into the microstructural changes associated with PCa. For example, extracellular matrix remodeling may contribute to the increased compartmental T_2 observed in C_2[12]. Lower compartmental T_2 values in C_3 may reflect hyperplasia-induced reductions in luminal space.[13] While the elevated compartmental T_2 observed in C_1 of csPCa patients may seem opposed to the known overall hypointense appearance of csPCa on T_2-weighted MRI, it is consistent with an increase in nuclear volume fraction that is typical of cancer cells[24].

We have previously shown that RSIrs is a useful quantitative DWI biomarker for csPCa at the voxel and patient levels[11,20,22]. Here, we evaluated whether incorporating compartmental T_2 values would improve csPCa discrimination. We demonstrated that T_2 effects have csPCa discriminatory value, as they showed higher AUC values compared to diffusion alone in both cohorts. However, consideration of compartmental T_2 did not significantly improve csPCa-detection performance over maximum RSIrs at the voxel- or patient-level. RSIrs already includes information related to global T_2 signal in the prostate (median signal in the whole prostate on the b=0 acquisition). It appears that this global T_2 assessment may contain sufficient information to normalize RSI diffusion signal and improve csPCa discrimination. This result suggests that compartmental T_2 mapping may not be worth the additional scan time and computation required.

Other advanced imaging techniques have also been used to measure T_2 in the prostate. LWI utilizes the unique T_2 relaxation rates associated with various components of prostate tissue to quantify the fractional volume of glandular lumen, denoted as luminal water fraction (LWF)[25]. This method takes advantage of the observed alterations in the composition of prostatic tissue in the presence of cancer and the Gleason grade of the

cancer for PCa diagnosis[26]. Hybrid multidimensional MRI (HM-MRI) exploits the interdependence of T_2 and ADC values to measure prostate volume fractions of the lumen, epithelium, and stroma[27]. Studies using LWI and HM-MRI demonstrate lower T_2 values in cancer lesions compared to normal prostate tissue with increasing Gleason Grade. The decrease in T_2 results from a decrease in luminal volume due to cellular hyperplasia[26,28]. This trend agrees with the decrease observed in this study of T_2 in compartment C_3 of patients with csPCa. This compartment reflects signal from freely diffusing water in the prostate, which we expect to find predominantly in luminal tissue and to be impacted by a reduction in luminal space. Prior work with HM-MRI showed that the decrease in luminal space is largely the result of epithelial tissue proliferation, indicated by an increase in the measured epithelial volume fraction[27]. Since RSI does not explicitly assign signal contributions to a particular tissue type, this aspect of HM-MRI is harder to align with the present study. However, we can be sure that the changes observed in the T_2 of compartment C_1 reflect, at least in part, an increase in the overall tissue cellularity[29]. Signal contributions in this compartment are also dependent upon the nuclear volume fraction of cells in the tissue[24], and the increase in the T_2 observed in C_1 of csPCa patients suggests an increase in nuclear volume fraction. Whole-mount histopathology data is currently being collected as part of an ongoing study to map changes in compartmental RSI signal to the histological restructuring of prostate tissue due to csPCa.

Future work will also evaluate larger patient cohorts to consider the potential impact of compartmental T_2 measurements on the prediction of csPCa grade and tumor extent with the RSI framework. Finally, an ongoing, prospective trial is evaluating the impact of RSIrs and compartmental T_2 on csPCa diagnosis in multiple centers and with multiple readers.

Limitations

The use of separate acquisitions and only two TEs may have limited the accuracy of voxel-wise compartmental T_2 measurements. Our study used two TEs for each cohort, where the lowest TE was 76 ms. Other quantitative MRI approaches use lower TEs (less

than 30 ms) for T_2 mapping[14,26]. The high *b*-values necessary to optimally estimate RSI C_1 are generally incompatible with very low TE on clinical scanners, so separate acquisitions would be required to evaluate the combination of optimal RSIrs and T_2 estimated with very low TE. Another limitation of this study is that our voxel-level data included only high-confidence csPCa and control categories, leaving little room for improvement over RSIrs for the voxel-level analysis[11].

Conclusion

T_2 mapping affords insights into characteristics of benign and cancerous prostate tissue, but we did not find compelling evidence that acquisitions with multiple TE is necessary for patient-level csPCa detection with RSI.

References

1. Leung DKW, Chiu PKF, Ng CF, Teoh JYC. Role of pre-biopsy multiparametric MRI in prostate cancer diagnosis: Evidence from the literature. *Turk J Urol*. 2021;47(Suppl 1):S65-S70. doi:10.5152/tud.2020.20360

2. de Rooij M, Hamoen EHJ, Fütterer JJ, Barentsz JO, Rovers MM. Accuracy of multiparametric MRI for prostate cancer detection: a meta-analysis. *AJR Am J Roentgenol*. 2014;202(2):343-351. doi:10.2214/AJR.13.11046

3. Schoots IG, Roobol MJ, Nieboer D, Bangma CH, Steyerberg EW, Hunink MGM. Magnetic resonance imaging-targeted biopsy may enhance the diagnostic accuracy of significant prostate cancer detection compared to standard transrectal ultrasound-guided biopsy: a systematic review and meta-analysis. *Eur Urol*. 2015;68(3):438-450. doi:10.1016/j.eururo.2014.11.037

4. Scott R, Misser SK, Cioni D, Neri E. PI-RADS v2.1: What has changed and how to report. *SA J Radiol*. 2021;25(1):2062. doi:10.4102/sajr.v25i1.2062

5. Demirel HC, Davis JW. Multiparametric magnetic resonance imaging: Overview of the technique, clinical applications in prostate biopsy and future directions. *Turk J Urol*. 2018;44(2):93-102. doi:10.5152/tud.2018.56056

6. Pickersgill NA, Vetter JM, Andriole GL, et al. Accuracy and Variability of Prostate Multiparametric Magnetic Resonance Imaging Interpretation Using the Prostate Imaging Reporting and Data System: A Blinded Comparison of Radiologists. *Eur Urol Focus*. 2020;6(2):267-272. doi:10.1016/j.euf.2018.10.008

7. Midiri F, Vernuccio F, Purpura P, Alongi P, Bartolotta TV. Multiparametric MRI and Radiomics in Prostate Cancer: A Review of the Current Literature. *Diagn Basel Switz*. 2021;11(10):1829. doi:10.3390/diagnostics11101829

8. Stabile A, Giganti F, Kasivisvanathan V, et al. Factors Influencing Variability in the Performance of Multiparametric Magnetic Resonance Imaging in Detecting Clinically Significant Prostate Cancer: A Systematic Literature Review. *Eur Urol Oncol*. 2020;3(2):145. doi:10.1016/j.euo.2020.02.005

9. Brunsing RL, Schenker-Ahmed NM, White NS, et al. Restriction spectrum imaging: An evolving imaging biomarker in prostate MRI: Prostate MRI with Restriction Spectrum Imaging: A Review. *J Magn Reson Imaging*. 2017;45(2):323-336. doi:10.1002/jmri.25419

10. Conlin CC, Feng CH, RodrÃ-guez-Soto AE, et al. *Improved Characterization of Diffusion in Normal and Cancerous Prostate Tissue through Optimization of the Restriction Spectrum Imaging Signal Model*. Radiology and Imaging; 2020. doi:10.1101/2020.03.27.20042069

11. Feng CH, Conlin CC, Batra K, et al. Voxel-level Classification of Prostate Cancer on Magnetic Resonance Imaging: Improving Accuracy Using FOUR-COMPARTMENT Restriction Spectrum Imaging. *J Magn Reson Imaging*. 2021;54(3):975-984. doi:10.1002/jmri.27623

12. White NS, McDonald CR, Farid N, et al. Diffusion-Weighted Imaging in Cancer: Physical Foundations and Applications of Restriction Spectrum Imaging. *Cancer Res*. 2014;74(17):4638-4652. doi:10.1158/0008-5472.CAN-13-3534

13. Hectors SJ, Said D, Gnerre J, Tewari A, Taouli B. Luminal Water Imaging: Comparison With Diffusion-Weighted Imaging (DWI) and PI-RADS for Characterization of Prostate Cancer Aggressiveness. *J Magn Reson Imaging*. 2020;52(1):271-279. doi:10.1002/jmri.27050

14. Chatterjee A, Bourne RM, Wang S, et al. Diagnosis of Prostate Cancer with Noninvasive Estimation of Prostate Tissue Composition by Using Hybrid Multidimensional MR Imaging: A Feasibility Study. *Radiology*. 2018;287(3):864-873. doi:10.1148/radiol.2018171130

15. EAU Guidelines on Prostate Cancer - Uroweb. Uroweb - European Association of Urology. Accessed October 16, 2023. https://uroweb.org/guidelines/prostate-cancer

16. Abdul Raheem R, Razzaq A, Beraud V, et al. Can a prostate biopsy be safely deferred on PI-RADS 1,2 or 3 lesions seen on pre-biopsy mp-MRI? *Arab J Urol*. 21(1):10-17. doi:10.1080/2090598X.2022.2119711

17. Reijnen JS, Marthinsen JB, Tysland AO, et al. Results from a PI-RADS-based MRI-directed diagnostic pathway for biopsy-naive patients in a non-university hospital. *Abdom Radiol N Y*. 2021;46(12):5639-5646. doi:10.1007/s00261-021-03249-8

18. Holland D, Kuperman JM, Dale AM. Efficient correction of inhomogeneous static magnetic field-induced distortion in Echo Planar Imaging. *NeuroImage*. 2010;50(1):175-183. doi:10.1016/j.neuroimage.2009.11.044

19. Paquin D, Levy D, Schreibmann E, Xing L. MULTISCALE IMAGE REGISTRATION.

20. Zhong AY, Digma LA, Hussain T, et al. Automated Patient-level Prostate Cancer Detection with Quantitative Diffusion Magnetic Resonance Imaging. *Eur Urol Open Sci*. 2023;47:20-28. doi:10.1016/j.euros.2022.11.009

21. Conlin CC, Karunamuni R, Hussain TS, et al. *Background Prostate Tissue Is Quantitatively Abnormal on MRI in Patients with Clinically Significant Prostate Cancer*. Radiology and Imaging; 2022. doi:10.1101/2022.10.12.22280855

22. Lui AJ, Kallis K, Zhong AY, et al. *ReIGNITE RT Boost: An International Study Testing the Accuracy and Feasibility of Using Restriction Spectrum Imaging (RSI) MRI to Guide Intraprostatic Tumor Target Volume for Radiotherapy Boost*. Oncology; 2022. doi:10.1101/2022.12.13.22283420

23. Kallis K, Conlin CC, Zhong AY, et al. *Comparison of Synthesized and Acquired High* b *-Value Diffusion-Weighted MRI for Detection of Prostate Cancer*. Radiology and Imaging; 2023. doi:10.1101/2023.02.17.23286100

24. White NS, Dale AM. Distinct effects of nuclear volume fraction and cell diameter on high b-value diffusion MRI contrast in tumors: Diffusion in Tumor Cells. *Magn Reson Med*. 2014;72(5):1435-1443. doi:10.1002/mrm.25039

25. Chatterjee A, Harmath C, Oto A. New prostate MRI techniques and sequences. *Abdom Radiol*. 2020;45(12):4052-4062. doi:10.1007/s00261-020-02504-8

26. Sabouri S, Chang SD, Savdie R, et al. Luminal Water Imaging: A New MR Imaging T2 Mapping Technique for Prostate Cancer Diagnosis. *Radiology*. 2017;284(2):451-459. doi:10.1148/radiol.2017161687

27. Lee GH, Chatterjee A, Karademir I, et al. Comparing Radiologist Performance in Diagnosing Clinically Significant Prostate Cancer with Multiparametric versus Hybrid Multidimensional MRI. *Radiology*. 2022;305(2):399-407. doi:10.1148/radiol.211895

28. Chatterjee A, Watson G, Myint E, Sved P, McEntee M, Bourne R. Changes in Epithelium, Stroma, and Lumen Space Correlate More Strongly with Gleason Pattern and Are Stronger Predictors of Prostate ADC Changes than Cellularity Metrics. *Radiology*. 2015;277(3):751-762. doi:10.1148/radiol.2015142414

29. Liss MA, White NS, Parsons JK, et al. MRI-Derived Restriction Spectrum Imaging Cellularity Index is Associated with High Grade Prostate Cancer on Radical Prostatectomy Specimens. *Front Oncol*. 2015;5. doi:10.3389/fonc.2015.00030